

LT scaling in depleted quantum spin ladders

S. Galeski,^{1,2,*} K. Yu. Povarov,¹ D. Blosser,¹ S. Gvasaliya,¹
R. Wawrzynczak,^{2,3} J. Ollivier,³ J. Gooth,² and A. Zheludev^{1,†}

¹Laboratory for Solid State Physics, ETH Zürich, 8093 Zürich, Switzerland

²Max Planck Institute for Chemical Physics of Solids, Nöthnitzer Strasse 40, 01187 Dresden, Germany

³Institut Laue-Langevin, 6 rue Jules Horowitz, 38042 Grenoble, France

(Dated: May 11, 2022)

Using a combination of neutron scattering, calorimetry, Quantum Monte Carlo (QMC) simulations and analytic results we uncover confinement effects in depleted, partially magnetized quantum spin ladders. We show that introducing non-magnetic impurities into magnetized spin ladders leads to the emergence of a new characteristic length L in the otherwise scale-free Tomonaga–Luttinger liquid (serving as the effective low-energy model). This results in universal LT scaling of staggered susceptibilities. Comparison of simulation results with experimental phase diagrams of prototypical spin ladder compounds DIMPY and BPCB yields excellent agreement.

Understanding the interplay of electron correlation and disorder is one of the central problems of condensed matter physics. The influence of disorder becomes crucial in one dimension where the non-trivial topology does not allow for quasi-particles to avoid even the smallest defects [1]. The impact of such interaction can be especially dramatic in gapless many-body 1D systems realizing a quantum critical Tomonaga–Luttinger Liquid (TLL) - a one dimensional analogue of the celebrated Fermi liquid [1–4]. Similarly to the latter, the TLL is characterized by the analogue of Fermi velocity v that sets the energy scale (conveniently expressed in units such as Kelvin), and additional exponent K reflecting the strength and type of interactions in the system.

A paradigmatic model for the study of the TLL physics is the simple $S = 1/2$ Heisenberg chain. Recent studies of site disorder in spin chain materials have shown that introduction of defects into the chain lattice effectively divides the liquid into finite pieces [5, 6]. Such segmentation has a profound effect on the low temperature properties of the TLL: the pure system, being in a quantum critical state is characterized by only a single energy scale — temperature T . Introduction of defects imposes a novel scale: the average distance between defects L and leads to discretization of the TLL energy levels with a v/L step [see Fig. 1(a)]. This in turn leads to the replacement of the original T -universality by an new LT -universality: all dynamic and thermodynamic observables become functions of the product LT only [6–8]. However, for the general anisotropic XXZ case such theoretical studies were performed only in $T = 0$ limit so far [9].

A central question in the study of defects in low dimensional quantum magnets is whether the LT scaling is a truly universal property of disordered TLLs, even when defects do not break the liquid’s continuity and for arbitrary TLL exponent K . The simplest realistic model allowing for the study of this problem is the depleted Heisenberg $S = 1/2$ ladder. Unlike the spin chain, it offers a much less restrictive geometry since removing one

	J_{\perp} (K)	J_{\parallel} (K)	J' (mK)	$g_{H\parallel a}$	ξ (lat. u.)	v (K)	K
DIMPY	9.5	16.74	75	2.13	6.3	22.04	1.23
BPCB	12.96	3.6	80	2.06	~ 0.8	3.94	0.93

TABLE I. Magnetic Hamiltonian constants of BPCB [12] and DIMPY [13] for rung, leg and interladder interaction and the g -factor [14, 15] for the relevant field direction. Also the corresponding correlation length ξ in the gapped phase, and TLL parameters at 8 T: Luttinger velocity v and dimensionless exponent K are given.

spin from the lattice does not break the ladder continuity, as shown Fig. 1. In addition, different interaction parameters K can be achieved in ladders with different rung and leg exchange coupling ratios J_{\perp}/J_{\parallel} , with strong leg ladders displaying attractive and strong rung ladders repulsive interactions [10]. This K -exponent is also tunable by the magnetic field, and is usually found from numeric simulations for a given system [11]. Thus, the depleted spin ladder magnets open up an avenue to explore the “dirty TLL” physics in the most generic, controlled, and tunable way.

In this Letter we experimentally and theoretically study the effect of spin depletion on two organometallic spin ladder materials: BPCB [12, 15–17] and DIMPY [13, 18–20]. Both of these materials are well established realizations of $S = 1/2$ Heisenberg ladder Hamiltonian and harbour an attractive (DIMPY) and repulsive (BPCB) TLL when magnetized [10, 12, 13]. The most relevant parameters of the materials are given in Table I [21]. Using inelastic neutron scattering we experimentally confirm the applicability of depleted ladder model to Zn^{2+} ($S = 0$) - substituted BPCB. Using a combination of QMC simulations [22], analytical calculations, and an extensive low temperature heat capacity survey we show that the LT scaling of staggered susceptibilities is a robust, universal property of disordered TLL regardless of the K parameter. Our findings suggest that such scaling persists even if the continuity of TLL remains preserved,

a situation inaccessible in the segmented spin chain settings studied before [6–9]. Thus, LT universality appears to be a generic property of “dirty” TLLs.

The samples were grown in house by the thermal gradient [(C₇H₁₀N)₂Cu_{1-z}Zn_zBr₄ DIMPY] and solvent evaporation [(C₅H₁₂N)₂Cu_{1-z}Zn_zBr₄ BPCB] methods, similar to the pristine materials [15, 18], with replacement of the relevant amount z of CuBr₂ by ZnBr₂. Both in specific heat and neutron scattering experiments we have used fully deuterated chemicals for growth of BPCB crystals. The Zn²⁺ content in the studied samples was verified using Micro X-ray fluorescence chemical analysis and independently crosschecked through comparison of low field magnetization measurements with QMC simulations. The DIMPY samples were already used in the previous study [23].

In a depleted spin ladder, at low magnetic fields the non-magnetic defects were shown to lead to the emergent clusters of staggered magnetization (“spin islands”), as typical for a gapped system [23, 24]. The effect of Zn substitution in DIMPY at low fields has been already thoroughly studied revealing that Zn-doped DIMPY is an excellent realization of a depleted strong leg spin ladder Hamiltonian [23]. However, despite the structural and chemical similarity between BPCB and DIMPY, an assumption that BPCB also realizes a depleted spin ladder Hamiltonian cannot be taken for granted. In order to verify that this is the case we have studied the emergent Zn-induced “spin island” degrees of freedom in the gapped phase of BPCB. Thanks to the short correlation length in BPCB, these “islands” are expected to exhibit no overlap for low Zn substitution levels and thus behave as uncorrelated paramagnetic impurities and scatter neutrons elastically. Their presence could thus be only detected as a magnetic field induced Zeeman resonance. The localized spin-1/2 degrees of freedom should appear as a non-dispersive level, very broad in momentum, centered at $\hbar\omega = g\mu_B\mu_0 H$. A similar kind of Zeeman resonance has been observed in a depleted Haldane material Y₂BaNi_{1-z}Mg_zO₅ [25].

In order to test those predictions we have performed an inelastic neutron spectroscopy study of 5 coaligned $z = 0.02$ BPCB crystals with total mass 0.9 g, at the IN5 time-of-flight spectrometer [26] (ILL, Grenoble) with a split-coil vertical magnet. Fig. 2(a,b) shows a comparison between magnetic neutron spectra collected at $T = 60$ mK in and in 0 T and 2.5 T with the magnetic field applied along the crystals b -axis. The data were collected with 2.2 and 1.2 meV incident energy, then treated with HORACE software [27]. Neutron intensity is shown as a function of energy transfer $\hbar\omega$ and momentum transfer along the leg direction Q_{\parallel} . The 0 T spectrum demonstrates that introduction of non-magnetic defects does not alter the magnon dispersion [28] in any obvious way compared with the pristine material. The dispersion itself is well-captured by the strong-rung limit

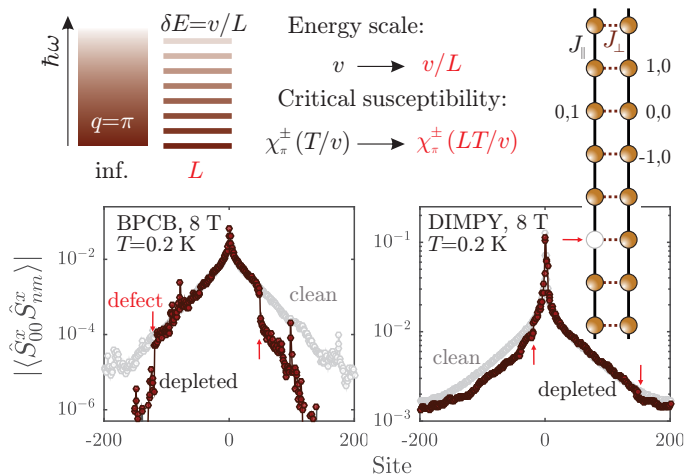


FIG. 1. (a) Origin of LT scaling in Tomonaga–Luttinger liquids. Finite-size effect results in equidistant discretization of the energy spectrum at critical wavevector and in effect to suppression of corresponding susceptibility. (b) A QMC simulation of the transverse two-spin correlator in a pure and depleted 400-site magnetized DIMPY and BPCB spin ladders. The two randomly placed defects in the ladder (shown by red arrows) are partially “transparent” to correlations.

expansion of the spin ladder model [29]. There are no novel low energy features visible over the magnet-related background, justifying the weakly correlated picture of the defects in BPCB, contrasting the case of DIMPY. In contrast at 2.5 T there appears a clearly distinguishable non-dispersive level at 0.3 meV [see Fig. 2(b,c)] — the expected resonance. The $S = 1$ magnon’s dispersion remains unchanged apart from splitting into three branches due to Zeeman effect. This is exactly the behavior one would expect from the depleted spin ladder with the parameters of BPCB. The availability of the “isolated island” analytic solution in the strong-rung limit with short correlations is very helpful, as the numeric simulations of spectral properties are extremely demanding in the presence of disorder. Thus, we are confident that the chemical substitution in both materials functions the same way (merely depleting the spin ladder) and further comparison of critical properties in high magnetic fields would be meaningful.

In magnetic fields strong enough to close the magnon gap, fate of the spin impurities is expected to change. Above the critical field the spin ladder enters the gapless TLL phase [1, 30]. The most distinct difference between TLLs realized in spin chain and magnetized spin ladders is that ladder lattices offer a much less restrictive geometry. Thus it can be expected that introduction of non-magnetic defects could induce a novel length scale into the problem without sacrificing the TLL continuity. To test if non-magnetic defects would remain at least partially transparent to spin correlations in magnetized spin ladders we have performed direct Quantum

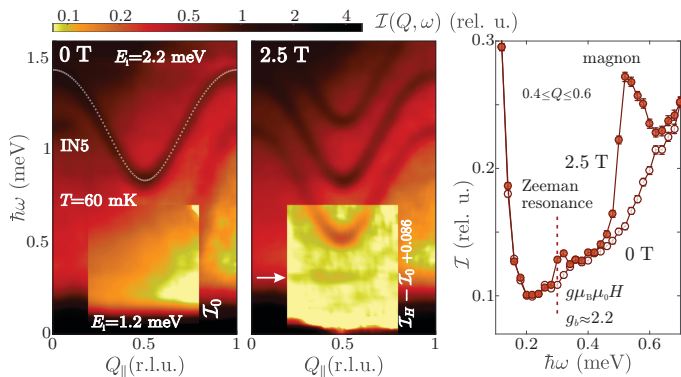


FIG. 2. (a,b) Magnetic neutron scattering intensity as a function of energy and momentum transfer (along the ladder leg) of depleted BPCB in 0 and 2.5 T. The spectra were taken using an incident neutron energy of 2.2 (in the main panels) and 1.2 meV (in the insets). For 2.5 T case inset shows the background-subtracted intensity; the arrow shows the position of the impurity-related scattering. Dashed line in 0 T panel is the reference magnon dispersion in clean BPCB [28]. (c) Intensity profiles $\mathcal{I}(\omega)$ near $Q_{\parallel} = 0.5$ r.l.u. Zeeman resonance at 0.3 meV is well visible in the magnetized case.

Monte Carlo (QMC) simulations of the transverse components of spin-spin correlations $\langle \hat{S}_{00}^x \hat{S}_{mn}^x \rangle$ on two ladder lattices with coupling constants resembling that of our target materials. The calculations have been performed using the `dirloop-sse` algorithm of the ALPS package [22, 31]. The results of those calculations displayed in Fig. 1 suggest that as naively expected, spin correlations can propagate along the ladder despite the presence of non-magnetic defects for both DIMPY and BPCB. Comparing the left and right panel of Fig. 1(b) reveal that defects suppress spin correlations much more efficiently in the case of the repulsive TLL realized in BPCB than in the attractive case of DIMPY.

In order to verify that introduction of defects that do not lead to segmentation of the TLL still leads to the presence of LT -scaling in the critical (transverse staggered χ_{π}^{\pm}) susceptibility of magnetized depleted ladders, we have performed another series of QMC simulations. Although the ALPS `dirloop-sse` algorithm [22, 31] does not give direct access to χ_{π}^{\pm} for magnetized systems, it does allow for the calculation of the static transverse correlation function $\langle S_{00}^+ S_{nm}^- \rangle$. While this quantity is in general not directly related to the susceptibility, in the case of TLL it can be shown that per mol of spins we have:

$$\chi_{\pi}^{\pm}(L, T) = \frac{N_A}{k_B} \frac{(g\mu_B)^2}{LT\mathcal{R}(K)} \sum_{n,m,k,l} (-1)^{n-m+k-l} \langle S_{nk}^+ S_{ml}^- \rangle, \quad (1)$$

with $\mathcal{R}(K)$ being a prefactor of the order of 1, that can be analytically derived [21].

Using the QMC results and Eq. (1) we have computed the staggered transverse susceptibility for a series of spin ladder lattices of 10, 20, 50, 100 and 200 rungs with coupling constants resembling those of DIMPY and BPCB, in 8 T field, and with the boundaries being open. The resulting susceptibilities are plotted in the inset of Fig. 3(a). However, as we can see, the simple $\chi_{\pi}^{\pm}(L, T) \times T$ product does not show apparent scaling as it would in the open boundaries Heisenberg spin chain case with $K = 1/2$ [7]. The temperature-related power law requires a modification here, and we argue that the generalized scaling relation should be [21]:

$$\chi_{\pi}^{\pm}(L, T) \propto \left(\frac{T}{v}\right)^{\frac{1}{2K}-2} F_K\left(\frac{LT}{v}\right), \quad (2)$$

with $F_K(x)$ being a K -parameterized single argument function. Once the data is replotted in the respective coordinates [Fig. 3(a)], the presence of scaling (2) in the low- T regime becomes apparent. This is consistent with the power law $T^{1/2K-2}$ for the thermodynamic limit [1]. At higher temperatures the behavior is non-TLL in general and the scaling breaks down.

To test the hypothesis that introducing random spin depletion also introduces a new length scale leading to LT scaling we have performed a second set of QMC simulations. Assuming the same coupling parameters and applied magnetic fields we have computed the susceptibilities for both ladder systems with 400 rungs and 1, 2, 4 and 6% spin depletion and averaged over 20 different random impurity distributions. The results of these calculations are displayed in Fig. 3(b). Strikingly despite some differences in overall shape of the curves compared to the finite length pieces, the susceptibilities in “depleted ladders” closely follow the derived scaling law.

These theoretical results would be best confirmed through a direct comparison with measurements of transverse staggered susceptibilities of several samples with different level of dilution. Although such measurements could be in principle carried out using inelastic neutron scattering, in practice it would be a formidable task. Another avenue for testing our QMC results can be provided through testing the ability of our target systems to achieve 3D ordering. One of the most spectacular ways spin depletion influences low temperature properties of quasi-1D magnets is through altering their ordering capabilities: in ultra pure site diluted SrCuO_2 samples the presence of less than 1% of impurities suppresses Néel ordering beyond experimental detection [6]. The mean field condition for magnetic ordering ties the ordering temperature, critical susceptibility and the strength of residual 3D couplings J' [30, 32, 33]:

$$\chi_{\pi}^{\pm}(T_N) = \frac{N_A}{k_B} \frac{(g\mu_B)^2}{J'}. \quad (3)$$

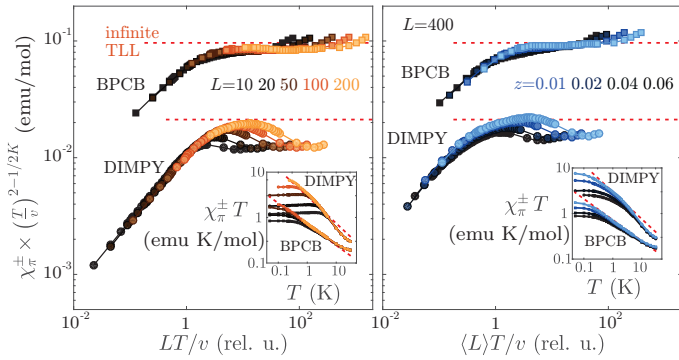


FIG. 3. Comparison of LT/v scaling properties of staggered susceptibilities in finite spin ladder segments and depleted spin ladders. Susceptibility is extracted from QMC data according to (1); simulations are done at 8 T field for coupling constants of DIMPY and BPCB. (a) Scaling of finite spin ladder segments with open boundary conditions. (b) Scaling of 400 rung diluted spin ladder lattices, here $L = \frac{1-z}{2z-z^2}$ is the average inter-defect distance. In both panels the dashed lines show the scaling law expected for the infinite system. Insets show the unscathed data.

This explains the strong suppression of T_N in depleted spin chains: addition of impurities effectively cuts them, truncating the spin-spin correlations and leading to depression of the relevant susceptibility. Eq. (3) defines the critical susceptibility magnitude that triggers long range ordering. Thus to confirm the validity of our QMC simulations we have calculated the full phase diagram of both pure and depleted DIMPY and BPCB for a direct comparison with experimental phase diagrams obtained from specific heat measurements. We would like to stress that the simulations and measurements are performed away from the critical fields, and so possible Bose-glass related phenomena [34] are not relevant.

The magnetic phase diagrams for all samples were determined through locating the maxima of the specific heat anomalies attributed to 3D ordering via fitting Lorentzian-like peak functions (details are shown in [21]). The specific heat measurements were performed in the Quantum Design PPMS dilution refrigerator equipped in a standard specific heat option and a 9 T superconducting magnet. Representative datasets after subtracting the nuclear spin contribution for samples with different Zn substitution level of both DIMPY and BPCB are shown in Fig. 4. Inspection of both datasets reveals that spin depletion apart from quickly suppressing magnetic order additionally leads to broadening of the specific heat anomalies. It was shown that such broadening can be an effect of weak random fields arising due to chemical disorder [35]. Indeed it can be expected that spin depletion of a single ladder not only decreases its staggered transverse susceptibility leading to the depression of T_N but also exerts an effective random field on the neighbouring ladders. Interestingly apart from altering the shape

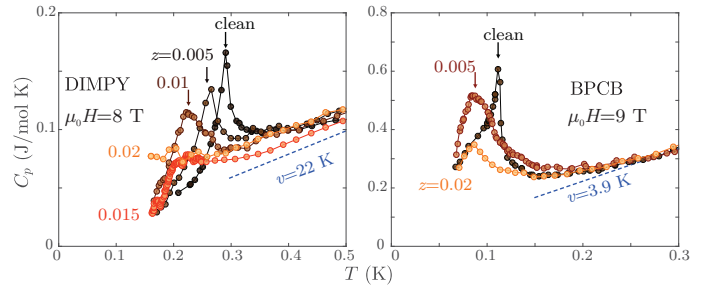


FIG. 4. Comparison of the spin dilution effect on the specific heat anomaly of DIMPY and BPCB measured at 8 and 9 T, respectively. Dashed lines show the expected TLL linear specific heat. Arrows mark the transition temperature.

and location of the specific heat anomaly spin depletion seems to have no influence on the high temperature specific heat. This simple observation suggests that although adding non-magnetic impurities changes the span of correlation functions it does not influence the spinon velocity v as $C_v^{\text{TLL}}(T) = R \frac{\pi}{6v} T$. Moreover, previous studies of equal-time correlations scaling in depleted chains [5] suggest that defects do not alter the exponent K either, in agreement with our QMC analysis.

To verify that our QMC procedure is reliable in computing physical properties of the relevant materials we have calculated the longitudinal uniform susceptibility which is a directly observable quantity. For comparison with simulations we have measured the susceptibility of both materials using the PPMS AC-susceptibility option at 8 T. As shown in the inset of Fig. 5(a) the agreement of the QMC result with experiment is excellent confirming the validity of our approach.

The first crucial step in simulating phase diagrams of depleted spin ladders is the determination of the inter ladder coupling constant J' . To do this we have calculated the transverse staggered susceptibility for pure 400 rung systems with periodic boundary conditions and then fitted Eq. (3) to the experimental specific heat data using J' as a fitting parameter, following the procedure of [13]. As a result we have established the interladder coupling to be 106mK and 110 mK for DIMPY and BPCB respectively, values slightly higher than previously obtained through a combined DMRG and field theory approach. Although estimating T_N for the case of depleted ladders from susceptibility calculations with similar level of averaging to those used for the scaling analysis qualitatively reproduce the experimental phase diagram, the predicted phase boundaries showed to be off by over 20% compared to the experimental results. In order to correct for the effect of under-averaging we have thus calculated the expected T_N for several fields averaging over 100 random impurity configurations. This allowed us to obtain predictions for T_N with excellent agreement with empirical data.

The final comparison of experimental and calculated

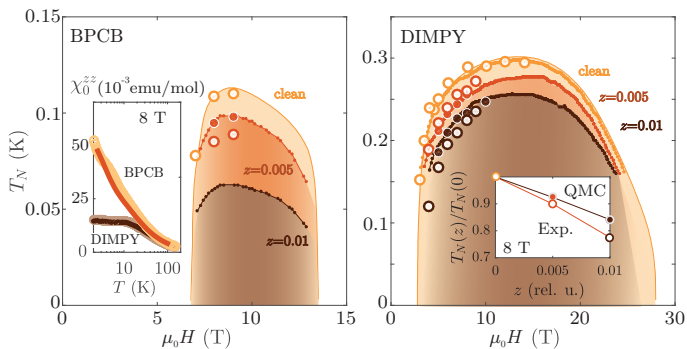


FIG. 5. Comparison of QMC simulation results with experimental phase diagrams obtained from specific heat: large solid circles mark points in the $H - T$ plane where the calculation was performed using 100 random impurity configurations; small circles are the rescaled results with 20 configurations. The large open circles represent results of heat capacity measurements. Thin line for the clean case is the DMRG-based mean field result. (a) The inset shows a comparison of simulated and measured uniform longitudinal magnetic susceptibility per spin of pure DIMPY and BPCB at 8 T (lines — QMC results, symbols are the measured values). (b) The inset shows a comparison of experimental and simulated values of T_N at 8 T.

phase diagrams is shown in the main panels of Fig. 5. For both materials the QMC result seems to accurately reproduce the phase diagrams for both pure and diluted samples. The excellent predictive power of our QMC calculation confirms that our simulation method can be used to accurately calculate $\chi_{\pi}^{\pm}(T)$ for a range of magnetic fields. This in turn reassures the validity of the LT scaling analysis in depleted spin ladders. Finally, we would like to note that in case of attractive TLL in DIMPY the ordered phase is much more resistant to defects compared to the case of repulsive TLL in BPCB. This seems to be the experimental consequence of spontaneous defect “healing” in an attractive TLL [36], also in line with the direct calculation of (small) correlation suppression in DIMPY case shown in Fig. 1(b).

Our results combined with Ref. [23] paint a full picture of the interplay of spin depletion and magnetic fields in spin ladders. At low magnetic fields $H < H_{c1}$ defects introduce packets of localized staggered magnetization that can give rise to a new emergent magnetic system if located densely enough to interact with one another. On the other hand at high fields $H > H_{c1}$ defects truncate the spin-spin correlation introducing a new length scale and introducing the new LT universality even when the TLL is not fully segmented. Those results suggests that the quantum critical state is in general susceptible to adjusting to externally imposed length scales such as disorder. We have verified that the LT scaling generally emerges in the presence of impurities for any degree of continuity and any Luttinger exponent K . Our analysis is expected to be directly transferable to other TLL sys-

tems such as nanowires, or the quantum Hall edge states. Another interesting possible application are the 1D disordered quantum magnets with charge degrees of freedom, such as $\text{Sr}_{14}\text{Cu}_{24}\text{O}_{41}$ [37] or BaFe_2S_3 [38]. It remains to be verified if our results will hold in these more complex situations.

This work was supported by the Swiss National Science Foundation, Division II. Part of the numerical simulations were performed on the ETH Zürich Euler cluster. We also acknowledge Mr. Jonathan Noky for his assistance in running the calculations on the computing cluster of Max Planck Institute for Chemical Physics of Solids, Dresden. We would like to thank Dr. D. Schmidiger (ETH Zürich) for his involvement at the early stage of the project, Dr. R. Chitra (ETH Zürich) and Dr. Tobias Meng (TU Dresden) for insightful discussions, and Dr. F. Alet (CNRS, Université Paul Sabatier Toulouse) for helpful advice on QMC techniques.

* Corresponding author: Stanislaw.Galeski@cpfs.mpg.de

† zhelud@ethz.ch; <https://www.neutron.ethz.ch/>

- [1] T. Giamarchi, *Quantum Physics in One Dimension* (Oxford University Press, 2003).
- [2] I. A. Zaliznyak, A glimpse of a Luttinger liquid, *Nat. Mat.* **4**, 273 (2005); B. Lake, D. A. Tennant, C. D. Frost, and S. E. Nagler, Quantum criticality and universal scaling of a quantum antiferromagnet., *Nat. Mater.* **4**, 329 (2005).
- [3] B. Lake, A. M. Tsvetlik, S. Notbohm, A. D. Tennant, T. G. Perring, M. Reehuis, C. Sekar, G. Krabbes, and B. Büchner, Confinement of fractional quantum number particles in a condensed-matter system, *Nat. Phys.* **6**, 50 (2010).
- [4] A. Zheludev, Quantum Critical Dynamics and Scaling in One-Dimensional Antiferromagnets, *J. Exp. Theor. Phys.* **131**, 34 (2020).
- [5] G. Simutis, S. Gvasaliya, M. Månsson, A. L. Chernyshev, A. Mohan, S. Singh, C. Hess, A. T. Savici, A. I. Kolesnikov, A. Piovano, T. Perring, I. Zaliznyak, B. Büchner, and A. Zheludev, Spin Pseudogap in Ni-Doped SrCuO_2 , *Phys. Rev. Lett.* **111**, 067204 (2013); G. Simutis, S. Gvasaliya, N. S. Beesetty, T. Yoshida, J. Robert, S. Petit, A. I. Kolesnikov, M. B. Stone, F. Bourdarot, H. C. Walker, D. T. Adroja, O. Sobolev, C. Hess, T. Masuda, A. Revcolevschi, B. Büchner, and A. Zheludev, Spin pseudogap in the $S = \frac{1}{2}$ chain material Sr_2CuO_3 with impurities, *Phys. Rev. B* **95**, 054409 (2017).
- [6] G. Simutis, M. Thede, R. Saint-Martin, A. Mohan, C. Baines, Z. Guguchia, R. Khasanov, C. Hess, A. Revcolevschi, B. Büchner, and A. Zheludev, Magnetic ordering in the ultrapure site-diluted spin chain materials $\text{SrCu}_{1-x}\text{Ni}_x\text{O}_2$, *Phys. Rev. B* **93**, 214430 (2016).
- [7] S. Eggert, I. Affleck, and M. D. P. Horton, Néel Order in Doped Quasi-One-Dimensional Antiferromagnets, *Phys. Rev. Lett.* **89**, 047202 (2002).
- [8] J. Sirker, S. Fujimoto, N. Laflorencie, S. Eggert, and I. Affleck, Thermodynamics of impurities in the anisotropic Heisenberg spin-1/2 chain, *J. Stat. Mech.*

- Theor. Exp. **2008**, P02015 (2008).
- [9] A. Bohrdt, K. Jägering, S. Eggert, and I. Schneider, Dynamic structure factor in impurity-doped spin chains, *Phys. Rev. B* **98**, 020402 (2018).
- [10] M. Jeong, D. Schmidiger, H. Mayaffre, M. Klanjšek, C. Berthier, W. Knafo, G. Ballon, B. Vignolle, S. Krämer, A. Zheludev, and M. Horvatić, Dichotomy between Attractive and Repulsive Tomonaga-Luttinger Liquids in Spin Ladders, *Phys. Rev. Lett.* **117**, 106402 (2016).
- [11] T. Hikihara and A. Furusaki, Spin correlations in the two-leg antiferromagnetic ladder in a magnetic field, *Phys. Rev. B* **63**, 134438 (2001).
- [12] P. Bouillot, C. Kollath, A. M. Läuchli, M. Zvonarev, B. Thielemann, C. Rüegg, E. Orignac, R. Citro, M. Klanjšek, C. Berthier, M. Horvatić, and T. Giamarchi, Statics and dynamics of weakly coupled antiferromagnetic spin- $\frac{1}{2}$ ladders in a magnetic field, *Phys. Rev. B* **83**, 054407 (2011).
- [13] D. Schmidiger, P. Bouillot, S. Mühlbauer, S. Gvasaliya, C. Kollath, T. Giamarchi, and A. Zheludev, Spectral and Thermodynamic Properties of a Strong-Leg Quantum Spin Ladder, *Phys. Rev. Lett.* **108**, 167201 (2012).
- [14] V. N. Glazkov, M. Fayzullin, Y. Krasnikova, G. Skoblin, D. Schmidiger, S. Mühlbauer, and A. Zheludev, ESR study of the spin ladder with uniform Dzyaloshinskii-Moriya interaction, *Phys. Rev. B* **92**, 184403 (2015).
- [15] B. R. Patyal, B. L. Scott, and R. D. Willett, Crystal-structure, magnetic-susceptibility, and EPR studies of bis(piperidinium)tetrabromocuprate(II): A novel monomer system showing spin diffusion, *Phys. Rev. B* **41**, 1657 (1990).
- [16] B. Thielemann, C. Rüegg, H. M. Rønnow, A. M. Läuchli, J.-S. Caux, B. Normand, D. Biner, K. W. Krämer, H.-U. Güdel, J. Stahn, K. Habicht, K. Kiefer, M. Boehm, D. F. McMorrow, and J. Mesot, Direct Observation of Magnon Fractionalization in the Quantum Spin Ladder, *Phys. Rev. Lett.* **102**, 107204 (2009).
- [17] B. Thielemann, C. Rüegg, K. Kiefer, H. M. Rønnow, B. Normand, P. Bouillot, C. Kollath, E. Orignac, R. Citro, T. Giamarchi, A. M. Läuchli, D. Biner, K. W. Krämer, F. Wolff-Fabris, V. S. Zapf, M. Jaime, J. Stahn, N. B. Christensen, B. Grenier, D. F. McMorrow, and J. Mesot, Field-controlled magnetic order in the quantum spin-ladder system (Hpip) $_2$ CuBr $_4$, *Phys. Rev. B* **79**, 020408 (2009); M. Klanjšek, H. Mayaffre, C. Berthier, M. Horvatić, B. Chiari, O. Piovesana, P. Bouillot, C. Kollath, E. Orignac, R. Citro, and T. Giamarchi, Luttinger liquid physics in the spin ladder material CuBr $_4$ (C $_5$ H $_{12}$ N) $_2$, *Phys. Status Solidi C* **247**, 656 (2010).
- [18] A. Shapiro, C. P. Landee, M. M. Turnbull, J. Jorner, M. Deumal, J. J. Novoa, M. A. Robb, and W. Lewis, Synthesis, structure, and magnetic properties of an antiferromagnetic spin-ladder complex: Bis (2, 3-dimethylpyridinium) tetrabromocuprate, *J. Am. Chem. Soc.* **129**, 952 (2007).
- [19] D. Schmidiger, P. Bouillot, T. Guidi, R. Bewley, C. Kollath, T. Giamarchi, and A. Zheludev, Spectrum of a Magnetized Strong-Leg Quantum Spin Ladder, *Phys. Rev. Lett.* **111**, 107202 (2013).
- [20] M. Jeong, H. Mayaffre, C. Berthier, D. Schmidiger, A. Zheludev, and M. Horvatić, Attractive Tomonaga-Luttinger Liquid in a Quantum Spin Ladder, *Phys. Rev. Lett.* **111**, 106404 (2013); K. Yu. Povarov, D. Schmidiger, N. Reynolds, R. Bewley, and A. Zheludev, Scaling of temporal correlations in an attractive Tomonaga-Luttinger spin liquid, *Phys. Rev. B* **91**, 020406 (2015).
- [21] See the Supplemental Material for the details of the experiment setup and data analysis, numeric simulations and their interpretation, and theoretical approach to the finite-size scaling.
- [22] B. Bauer, L. D. Carr, H. G. Evertz, A. Feiguin, J. Freire, S. Fuchs, L. Gamper, J. Gukelberger, E. Gull, S. Guertler, *et al.*, The ALPS project release 2.0: open source software for strongly correlated systems, *J. Stat. Mech. Theor. Exp.* **2011**, P05001 (2011).
- [23] D. Schmidiger, K. Yu. Povarov, S. Galeski, N. Reynolds, R. Bewley, T. Guidi, J. Ollivier, and A. Zheludev, Emergent Interacting Spin Islands in a Depleted Strong-Leg Heisenberg Ladder, *Phys. Rev. Lett.* **116**, 257203 (2016).
- [24] H.-J. Mikeska, U. Neugebauer, and U. Schollwöck, Spin ladders with nonmagnetic impurities, *Phys. Rev. B* **55**, 2955 (1997); M. Sigrist and A. Furusaki, Low-Temperature Properties of the Randomly Depleted Heisenberg Ladder, *J. Phys. Soc. Jpn.* **65**, 2385 (1996); A. Lavaré, G. Roux, and N. Laflorencie, Magnetic responses of randomly depleted spin ladders, *Phys. Rev. B* **88**, 134420 (2013).
- [25] M. Kenzelmann, G. Xu, I. A. Zaliznyak, C. Broholm, J. F. DiTusa, G. Aeppli, T. Ito, K. Oka, and H. Takagi, Structure of end states for a haldane spin chain, *Phys. Rev. Lett.* **90**, 087202 (2003).
- [26] J. Ollivier and H. Mutka, IN5 cold neutron time-of-flight spectrometer, prepared to tackle single crystal spectroscopy, *J. Phys. Soc. Jap.* **80**, SB003 (2011).
- [27] R. A. Ewings, A. Buts, M. D. Le, J. van Duijn, I. Bustinduy, and T. G. Perring, HORACE: Software for the analysis of data from single crystal spectroscopy experiments at time-of-flight neutron instruments, *Nucl. Instrum. Methods Phys. Res., Sect. A* **834**, 132 (2016).
- [28] D. Blosser, V. K. Bhartiya, D. J. Voneshen, and A. Zheludev, $z = 2$ Quantum Critical Dynamics in a Spin Ladder, *Phys. Rev. Lett.* **121**, 247201 (2018); Origin of magnetic anisotropy in the spin ladder compound (C $_5$ H $_{12}$ N) $_2$ CuBr $_4$, *Phys. Rev. B* **100**, 144406 (2019).
- [29] M. Reigrotzki, H. Tsunetsugu, and T. M. Rice, Strong-coupling expansions for antiferromagnetic Heisenberg spin-one-half ladders, *J. Phys.:Cond. Mat.* **6**, 9235 (1994).
- [30] T. Giamarchi and A. M. Tsvelik, Coupled ladders in a magnetic field, *Phys. Rev. B* **59**, 11398 (1999).
- [31] A. W. Sandvik, Stochastic series expansion method with operator-loop update, *Phys. Rev. B* **59**, R14157 (1999); F. Alet, S. Wessel, and M. Troyer, Generalized directed loop method for quantum Monte Carlo simulations, *Phys. Rev. E* **71**, 036706 (2005).
- [32] H. J. Schulz, Dynamics of Coupled Quantum Spin Chains, *Phys. Rev. Lett.* **77**, 2790 (1996).
- [33] C. Yasuda, S. Todo, K. Hukushima, F. Alet, M. Keller, M. Troyer, and H. Takayama, Néel Temperature of Quasi-Low-Dimensional Heisenberg Antiferromagnets, *Phys. Rev. Lett.* **94**, 217201 (2005).
- [34] K. Trinh and S. Haas, Bond disorder in even-leg Heisenberg ladders, *Phys. Rev. B* **87**, 075137 (2013).
- [35] E. Wulf, S. Mühlbauer, T. Yankova, and A. Zheludev, Disorder instability of the magnon condensate in a frustrated spin ladder, *Phys. Rev. B* **84**, 174414 (2011).

- [36] C. L. Kane and M. P. A. Fisher, Transport in a one-channel Luttinger liquid, *Phys. Rev. Lett.* **68**, 1220 (1992).
- [37] G. Blumberg, P. Littlewood, A. Gozar, B. S. Dennis, N. Motoyama, H. Eisaki, and S. Uchida, Sliding density wave in $\text{Sr}_{14}\text{Cu}_{24}\text{O}_{41}$ ladder compounds, *Science* **297**, 584 (2002); S. Sahling, G. Remenyi, C. Paulsen, P. Monceau, V. Saligramam, C. Marin, A. Revcolevschi, L. P. Regnault, S. Raymond, and J. E. Lorenzo, Experimental realization of long-distance entanglement between spins in antiferromagnetic quantum spin chains, *Nature Phys.* **11**, 255 (2015).
- [38] H. Takahashi, A. Sugimoto, Y. Nambu, T. Yamauchi, Y. Hirata, T. Kawakami, M. Avdeev, K. Matsubayashi, F. Du, C. Kawashima, H. Soeda, S. Nakano, Y. Uwatoko, Y. Ueda, T. J. Sato, and K. Ohgushi, Pressure-induced superconductivity in the iron-based ladder material BaFe_2S_3 , *Nature Mat.* **14**, 1008 (2015); Y. Hirata, S. Maki, J.-i. Yamaura, T. Yamauchi, and K. Ohgushi, Effects of stoichiometry and substitution in quasi-one-dimensional iron chalcogenide BaFe_2S_3 , *Phys. Rev. B* **92**, 205109 (2015).

Supplemental Material for “*LT* scaling in depleted quantum spin ladders”

S. Galeski,^{1,2,*} K. Yu. Povarov,¹ D. Blosser,¹ S. Gvasaliya,¹
R. Wawrzynczak,^{2,3} J. Ollivier,³ J. Gooth,² and A. Zheludev^{1,†}

¹*Laboratory for Solid State Physics, ETH Zürich, 8093 Zürich, Switzerland*

²*Max Planck Institute for Chemical Physics of Solids, Nöthnitzer Strasse 40, 01187 Dresden, Germany*

³*Institut Laue-Langevin, 6 rue Jules Horowitz, 38042 Grenoble, France*

(Dated: May 11, 2022)

In this Supplemental Material we discuss the possibility of extracting the transverse staggered susceptibility of the magnetized ladder χ_{π}^{\pm} from the QMC data and the attempt to analytically describe such using the concept of universality and *LT*-scaling for the finite segments. A comparison between the numeric, analytical, and experimental results for the depleted ladders is also given. We also discuss the inelastic neutron scattering experiment and the treatment of specific heat data in some more details.

CONTENTS

I. Phase diagrams of depleted ladders	1
II. Inelastic neutron scattering experiment	2
III. Quantum Monte Carlo simulations	2
IV. Extracting the transverse staggered susceptibility	3
A. Fluctuation-Dissipation Theorem and Kramers–Kronig relations	3
B. Application to the Tomonaga–Luttinger Liquid	4
C. Finite-size applicability	4
V. Finite-size scaling of transverse staggered susceptibility	5
A. Eggert-Affleck-Horton recipe	5
1. Basic ideas	5
2. Dimensionless	6
B. Generalization to the anisotropic case	6
1. Our assumptions	6
2. Universal scaling	8
VI. Universal susceptibility vs numerics and experiment	8
A. The QMC data and the pristine TLL description	8
B. Scaled QMC data and the scaling ansatz	9
C. The scaling ansatz and the measured phase diagrams	9
References	11

I. PHASE DIAGRAMS OF DEPLETED LADDERS

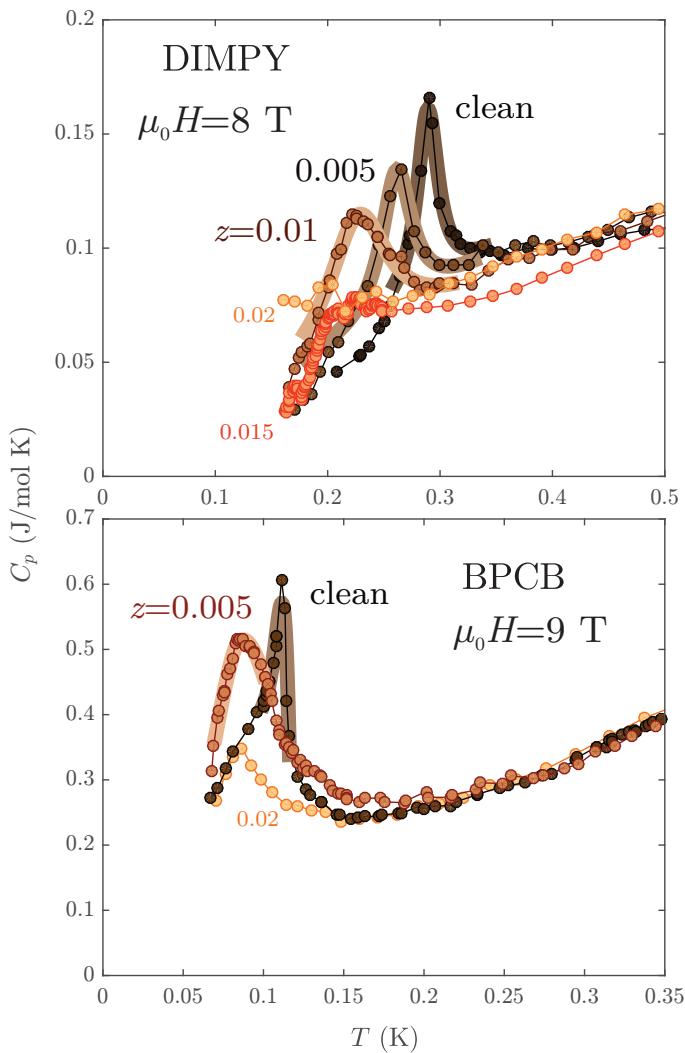
The extensive survey of low temperature specific heat of depleted DIMPY and BPCB allows to compile effective phase diagrams relating the transition temperature, spin depletion and magnetic field. Due to the disorder induced broadening of the transitions and the small data density precise determination of the transition temperature through direct inspection of the specific heat curves seems to be rather difficult. In order to overcome this difficulty we have extracted the critical temperature through fitting an empirical “peak function” composed of two Lorentzian-like functions. One of them is multiplied by T in order to account for the asymmetric appearance of the specific heat anomalies:

$$P(T) = \frac{a_1}{(T - T_N)^2 + \gamma_1} + \frac{a_2 T}{(T - T_N)^2 + \gamma_2} \quad (\text{S.1})$$

Example results of the fitting procedure is shown in Fig. 1. The fits obtained in the case of DIMPY allow to extract the value of T_N quite precisely. In the case of BPCB extracting T_N proved to be more difficult due to the complex shape of the specific heat anomalies. Although a satisfactory overlap of the experimental data with the model was obtained in the close vicinity of T_N , in the case of the 0.5% Zn sample this result should be treated with some prudence due to the possible influence of the anomaly tentatively attributed to nuclear specific heat. Despite this complication a careful subtraction of the specific heat curve of the 2% Zn substituted d-BPCB allows to estimate with high confidence that the presence of the additional ordering anomaly should not affect the extracted value of T_c of the Cu ions by more than 5-6%.

* Corresponding author: Stanislaw.Galeski@cpfs.mpg.de

† zhelud@ethz.ch; <https://www.neutron.ethz.ch/>



SUPP. FIG. 1. Eq. (S.1) [solid lines] was used to fit the specific heat data [points] in the vicinity of T_N in order to systematically extract the critical temperature from experimental data.

II. INELASTIC NEUTRON SCATTERING EXPERIMENT

The inelastic neutron scattering experiment was performed on the time-of-flight spectrometer IN5 at Institute Laue-Lagnevin, Grenoble, France. The sample consisted of five coaligned deuterated BPCB crystals with 2% Zn substitution, with total mass of the assembly being nearly 0.9 g. Crystals were mounted on the aluminum sampleholder with \mathbf{b} axis being vertical. The sampleholder was installed in a ^3He - ^4He dilution cryostat equipped with a split-coil vertical 2.5 T magnet. At the fields of both 0 and 2.5 T the experiment was performed in high resolution ($E_i = 1.2$ meV, δE 20 μeV FWHM) and low resolution ($E_i = 2.2$ meV, δE 45 μeV) modes. In both modes the sample was rotated by 150° with a 2° step. Neutron exposure time was nearly 35 minutes at every frame.

	DIMPY	BPCB
J_{\parallel} (K)	16.74 [3]	3.6 [4]
J_{\perp} (K)	9.5 [3]	12.96 [4]
J' (mK)	75 [3]	80 [4]
g_a	2.13 [5]	2.06 [6]
ξ (a units)	6.3 [7]	0.8 [8]
Simulated H (T)	8	8
K	1.23 [3]	0.93 [4]
v (K)	22.04 [3]	3.94 [4]
A_x	0.1891 [3]	0.1581 [4]
$\frac{1}{2K}$	-2	-1.59
\mathcal{R}	1.17	1.35

TABLE I. Basic Hamiltonian parameters of DIMPY and BPCB along with the relevant parameters of the Tomonaga-Luttinger liquid description in the 8 T magnetic field.

The neutron intensities measured at a given momentum transfer \mathbf{Q} and energy transfer $\hbar\omega$ are directly proportional to $\sum_{\alpha,\beta}(1 - Q^\alpha Q^\beta / |\mathbf{Q}|^2) \mathcal{S}^{\alpha\beta}(\mathbf{Q}, \omega)$. The measured dynamic structure factors $\mathcal{S}^{\alpha\beta}(\mathbf{Q}, \omega)$ are the Fourier transforms of the corresponding correlation functions:

$$\mathcal{S}^{\alpha\beta}(\mathbf{Q}, \omega) = \frac{1}{2\pi\hbar} \int_{-\infty}^{+\infty} \langle \hat{S}^\alpha(\mathbf{Q}, 0) \hat{S}^\beta(-\mathbf{Q}, t) \rangle e^{-i\omega t} dt \quad (\text{S.2})$$

The full dataset at each particular field and E_i is thus the intensity $\mathcal{I}(\mathbf{Q}, \omega)$, with $\mathbf{Q} = h\mathbf{a}^* + k\mathbf{b}^* + l\mathbf{c}^*$, being within the $(h, 0, l)$ plane predominantly. The collected data was projected onto the ladder direction \mathbf{a} . Thus, in Fig. 2 of the main text the intensity is shown as the function of momentum transfer along the ladder $Q_{\parallel} = (\mathbf{Q} \cdot \mathbf{a})/2\pi$ only.

III. QUANTUM MONTE CARLO SIMULATIONS

The Quantum Monte-Carlo simulations have been performed by means of Stochastic Series Expansion algorithm (`dirloop-sse`) of the ALPS library [1, 2]. The calculations were carried out on Euler cluster (ETH Zürich) and on the computing cluster of Max Planck Institute for Chemical Physics of Solids, Dresden. A thermalization of 10^6 was used, with $5 \cdot 10^4$ cycles per point. For the 400-rung depleted ladder model an averaging between 20 disorder configurations was done.

In Table I all the relevant parameters for both DIMPY and BPCB are summarized. Only J_{\perp} , J_{\parallel} , and the magnetic field strength are the input parameters of the simulations.

IV. EXTRACTING THE TRANSVERSE STAGGERED SUSCEPTIBILITY

In this section we will show that as long as the TLL-type universality holds in the system, it is possible to reliably estimate the static susceptibility from the equal-time correlations alone, without explicitly calculating the time-dependent ones.

A. Fluctuation-Dissipation Theorem and Kramers–Kronig relations

The `dirloop-sse` algorithm from the ALPS software provides access to the *equal time spin-spin correlation function*:

$$\begin{aligned} \mathcal{C}^{xx}(nk, ml) &= \frac{3}{S(S+1)} \langle\langle \hat{S}_{nk}^x \hat{S}_{ml}^x \rangle\rangle \\ &= 4 \langle\langle \hat{S}_{nk}^x(0) \hat{S}_{ml}^x(0) \rangle\rangle = 2 \langle\langle \hat{S}_{nk}^+(0) \hat{S}_{ml}^-(0) \rangle\rangle \end{aligned} \quad (\text{S.3})$$

Here the double angular brackets $\langle\langle \hat{A} \rangle\rangle$ stand for the statistical average $\text{Tr}(\hat{\rho} \hat{A})$, where $\hat{\rho}$ is the density matrix of the system.

For mapping the ladder onto the TLL we place the pseudospin objects \hat{s}_n on each rung:

$$\mathcal{S}_\pi^\pm(\omega) = \int_{-\infty}^{+\infty} \langle\langle \hat{s}^+(\pi, 0) \hat{s}^-(0, t) \rangle\rangle e^{-i\omega t} dt = \int_{-\infty}^{+\infty} \sum_{n,m} \langle\langle \hat{s}_n^+(0) \hat{s}_m^-(t) \rangle\rangle (-1)^{n-m} e^{-i\omega t} dt \quad (\text{S.9})$$

The spin dynamic structure factor is related to the *dissipative part of the susceptibility* via the *fluctuation-dissipation theorem*:

$$\chi_\pi^{\pm''}(\omega) = \frac{\pi(g\mu_B)^2}{L} [1 - e^{-\hbar\omega/k_B T}] \mathcal{S}_\pi^\pm(\omega) \quad (\text{S.10})$$

This susceptibility is defined per rung, hence the ladder length L in the denominator.

$$\chi_\pi^{\pm'} = \frac{1}{\pi} \mathcal{P} \int_{-\infty}^{+\infty} \frac{\chi_\pi^{\pm''}(\Omega)}{\Omega} d\Omega = \frac{(g\mu_B)^2}{L} \mathcal{P} \int_{-\infty}^{+\infty} \frac{[1 - e^{-\hbar\Omega/k_B T}]}{\Omega} \mathcal{S}_\pi^\pm(\Omega) d\Omega \quad (\text{S.12})$$

This is the rigorous formula recovering the *Van Vleck*

$$\hat{S}_{nk}^z = \frac{1}{4} + \frac{1}{2} \hat{s}_n^z \quad \text{and} \quad \hat{S}_{nk}^\pm = \frac{(-1)^k}{\sqrt{2}} \hat{s}_n^\pm \quad (\text{S.4})$$

For the pseudospins the following *equal time spin structure factor* would be relevant:

$$\mathcal{S}_\pi^\pm = \sum_{n,m} \langle\langle \hat{s}_n^+ \hat{s}_m^- \rangle\rangle (-1)^{n-m} \quad (\text{S.5})$$

As $\langle\langle \hat{s}_n^+ \hat{s}_m^- \rangle\rangle = \langle\langle (\hat{S}_{n1}^x - \hat{S}_{n2}^x)(\hat{S}_{m1}^x - \hat{S}_{m2}^x) \rangle\rangle$, we can relate this structure factor to the results of the numeric calculation:

$$\mathcal{S}_\pi^\pm = \sum_{n,m,k,l} (-1)^{n-m+l-k} \langle\langle \hat{S}_{nk}^x \hat{S}_{ml}^x \rangle\rangle \quad (\text{S.6})$$

$$= \frac{1}{4} \sum_{n,m,k,l} (-1)^{n-m+l-k} \mathcal{C}^{xx}(nk, ml) \quad (\text{S.7})$$

An alternative way to define the equal time structure factor is to frequency-integrate the complete *spin dynamic structure factor*:

$$\mathcal{S}_\pi^\pm = \int_{-\infty}^{+\infty} \mathcal{S}_\pi^\pm(\omega) d(\hbar\omega), \quad (\text{S.8})$$

that is:

Finally, the *reactive part of the susceptibility* can be obtained with the help of *Kramers–Kronig relations*:

$$\chi_\pi^{\pm'}(\omega) = \frac{1}{\pi} \mathcal{P} \int_{-\infty}^{+\infty} \frac{\chi_\pi^{\pm''}(\Omega)}{\Omega - \omega} d\Omega \quad (\text{S.11})$$

The static $\omega = 0$ limit of the susceptibility is thus:

part of the isothermal susceptibility. In the present case

this is the only term constituting the susceptibility of interest $\chi_\pi^\pm(T) = 2\chi_\pi^\pm$ (factor of 2 is from the fact that there are 2 spins per rung).

B. Application to the Tomonaga–Luttinger Liquid

We would like to start with the discussion of the infinite size system (the clean case with $L \rightarrow \infty$). Let us have a look at the Luttinger liquid dynamic structure factor at $q = \pi$ and at a finite temperature. It has a remarkable *universal* form:

$$\mathcal{S}_\pi^\pm(\omega) = \frac{A_x L}{\pi} (T/v)^{1/2K-2} \Phi\left(\frac{\hbar\omega}{k_B T}\right) \quad (\text{S.13})$$

Here A_x is some non-universal prefactor, and the scaling function that also depends on the Luttinger exponent K is:

$$\Phi(x) = \frac{1}{1-e^{-x}} \text{Im} \left[\left(\frac{\Gamma(1/8K - ix/4\pi)\Gamma(1 - 1/4K)}{\Gamma(1 - 1/8K - ix/4\pi)} \right)^2 \right] \quad (\text{S.14})$$

Another quantity of interest is the equal time structure factor, that is:

$$\mathcal{S}_\pi^\pm = \frac{A_x L}{\pi} \int_{-\infty}^{+\infty} (T/v)^{1/2K-2} \Phi\left(\frac{\hbar\omega}{k_B T}\right) d(\hbar\omega) = \frac{A_x L}{\pi} (T/v)^{1/2K-1} \int_{-\infty}^{+\infty} \Phi(x) dx \quad (\text{S.15})$$

What we have to compare is \mathcal{S}_π^\pm and the value of Kramers–Kronig integral (S.12):

$$L^{-1} \int_{-\infty}^{+\infty} \frac{A_x L}{\pi} \frac{1 - e^{-\hbar\Omega/k_B T}}{\Omega} \mathcal{S}_\pi^\pm(\Omega) d\Omega = \frac{A_x}{\pi} (T/v)^{1/2K-2} \int_{-\infty}^{+\infty} \frac{1 - e^{-\hbar\Omega/k_B T}}{\hbar\Omega/k_B T} \Phi\left(\frac{\hbar\Omega}{k_B T}\right) d(\hbar\Omega/k_B T) \quad (\text{S.16})$$

Thus, there exists a temperature-independent ratio:

$$\mathcal{R}(K) = \frac{2k_B^{-1}(g\mu_B)^2 \mathcal{S}_\pi^\pm}{LT\chi_\pi^\pm} = \frac{\int_{-\infty}^{+\infty} \Phi(x) dx}{\int_{-\infty}^{+\infty} \frac{1-e^{-x}}{x} \Phi(x) dx} \quad (\text{S.17})$$

For a given K this is just a number! Hence one can es-

tablish the exact correspondence between the staggered transverse susceptibility and the equal-time structure factor. The resulting way to relate the staggered transverse susceptibility *per spin* and the outcome of QMC calculation is:

$$\chi_\pi^\pm = \frac{k_B^{-1}(g\mu_B)^2}{2LT \times \mathcal{R}(K)} \sum_{n,m,k,l} (-1)^{n-m+l-k} \mathcal{C}^{xx}(nk, ml), \quad (\text{S.18})$$

with the Luttinger exponent $K(H)$ being the calibrated function of the static longitudinal magnetic field for each particular incarnation (DIMPY or BPCB) of the ladder model. As one can see from the Figure 2, the value of \mathcal{R} is around 1.5 for the K 's of interest.

C. Finite-size applicability

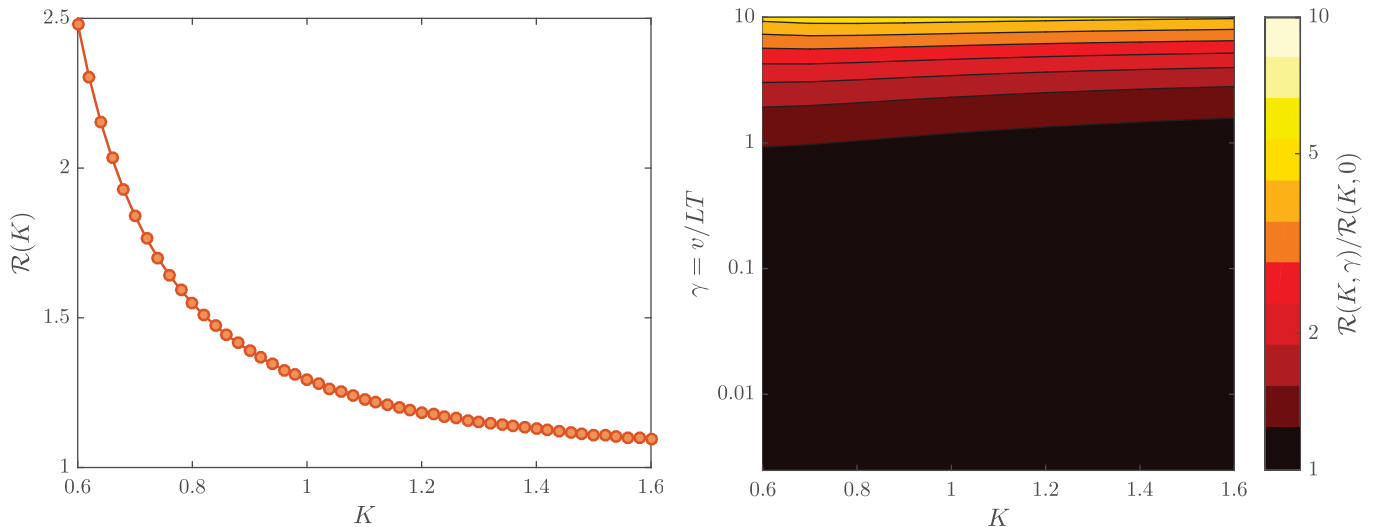
Now we can turn to the discussion of the depleted systems. The corresponding modification of the structure

factor (S.13) is:

$$\mathcal{S}_{xx}(\pi, \omega) = A_x (T/v)^{1/2K-2} \Phi\left(\frac{\hbar\omega}{k_B T}\right) \mathcal{F}\left(\frac{\Delta}{\hbar\omega}\right) \quad (\text{S.19})$$

The *envelope function* describing the missing due to depletion spectral weight at low energies (the pseudogap) can be approximated as:

$$\mathcal{F}(y) = \frac{y^2}{\sinh(y)^2}, \quad \Delta \simeq k_B v / \tilde{L} \quad (\text{S.20})$$



SUPP. FIG. 2. Left: The ratio (S.17) for the infinite length case. Right: The relative change due to the finite-size effects (S.21).

Such form of envelope function was used, for instance, in the discussion of dynamics of the depleted spin chain [9]. Remarkably, it is temperature independent, and it accounts simply for the discreteness of the spectrum in the finite-sized segments. Here v is the Luttinger velocity (setting the overall energy scale of a problem) and the parameter \tilde{L} can be understood as the typical, or average, segment length. The ratio \mathcal{R} , corresponding to the modified dynamic structure factor can be straightforwardly evaluated, and it will depend on the “magic” finite-size scaling parameter $\gamma = \frac{v}{LT}$. This is due to the fact that $\mathcal{F}\left(\frac{v}{\omega\tilde{L}}\right) = \mathcal{F}\left(\frac{\gamma}{\omega/T}\right)$. Thus, we need to evaluate:

$$\mathcal{R}(K, \gamma) = \frac{\int_{-\infty}^{+\infty} \Phi(x) \mathcal{F}\left(\frac{\gamma}{x}\right) dx}{\int_{-\infty}^{+\infty} \frac{1-e^{-x}}{x} \Phi(x) \mathcal{F}\left(\frac{\gamma}{x}\right) dx} \quad (\text{S.21})$$

The result is shown in Fig. 2. The conclusion is, finite-size effects can be neglected as long as $v/\tilde{L} \lesssim T$, that is mostly the case in our calculations. The “clean” prefactor $\mathcal{R}(K)$ can be used also for the depleted ladders, and Eq. (S.18) holds.

V. FINITE-SIZE SCALING OF TRANSVERSE STAGGERED SUSCEPTIBILITY

In this section we propose the *ansatz* to derive the transverse staggered susceptibility of a magnetized TLL. For the sake of brevity and clearness we omit the factors μ_0 , $g\mu_B$, and k_B here, to recover them at the final stages of our calculation.

A. Eggert-Affleck-Horton recipe

1. Basic ideas

We would like to start with the reminder for the isotropic $S = 1/2$ chain at zero field as formulated by Eggert, Affleck and Horton in Ref. [10]. We attempt to calculate the ordering temperature in the mean-field ensemble of chain segments. The distribution of the segment lengths corresponds to randomly placed chain breaks with z being the impurity concentration.

As the first step we calculate the single-segment staggered susceptibility, assuming it to be long enough for “Luttinger Liquid in a box” approach to be applicable. The staggered susceptibility in the isotropic case is:

$$\chi_{\pi}^{\pm}(L, T) = 2\chi_{\pi}^{zz}(L, T) = \frac{2}{L} \int_0^{1/T} d\tau \iint_0^L dx dy G(x, y, \tau) \quad (\text{S.22})$$

It is defined via the Green function:

$$G(x, y, \tau) = A_z \frac{\pi}{4L} \frac{\partial_x \theta_1(0, e^{-\frac{\pi\gamma}{2}})}{\sqrt{\theta_1\left(\frac{\pi x}{L}, \exp\left(-\frac{\pi\gamma}{2}\right)\right) \theta_1\left(\frac{\pi y}{L}, \exp\left(-\frac{\pi\gamma}{2}\right)\right)}} [G^+(x, y, \tau) - G^-(x, y, \tau)] \quad (\text{S.23})$$

where

$$G^+(x, y, \tau) = \frac{\theta_{2,3}(\pi \frac{x-y}{L}, e^{-\pi\gamma})}{\theta_{2,3}(0, e^{-\pi\gamma})} \sqrt{\frac{\theta_1(\frac{\pi}{2} \frac{x+y+i\tau}{L}, e^{-\frac{\pi\gamma}{2}}) \theta_1(\frac{\pi}{2} \frac{x+y-i\tau}{L}, e^{-\frac{\pi\gamma}{2}})}{\theta_1(\frac{\pi}{2} \frac{x-y+i\tau}{L}, e^{-\frac{\pi\gamma}{2}}) \theta_1(\frac{\pi}{2} \frac{x-y-i\tau}{L}, e^{-\frac{\pi\gamma}{2}})}}, \quad (\text{S.24})$$

and

$$G^-(x, y, \tau) = \frac{\theta_{2,3}(\pi \frac{x+y}{L}, e^{-\pi\gamma})}{\theta_{2,3}(0, e^{-\pi\gamma})} \sqrt{\frac{\theta_1(\frac{\pi}{2} \frac{x-y+i\tau}{L}, e^{-\frac{\pi\gamma}{2}}) \theta_1(\frac{\pi}{2} \frac{x-y-i\tau}{L}, e^{-\frac{\pi\gamma}{2}})}{\theta_1(\frac{\pi}{2} \frac{x+y+i\tau}{L}, e^{-\frac{\pi\gamma}{2}}) \theta_1(\frac{\pi}{2} \frac{x+y-i\tau}{L}, e^{-\frac{\pi\gamma}{2}})}}. \quad (\text{S.25})$$

The important scaling parameter γ is defined as $\gamma = \frac{v}{LT}$ (with $v = \pi J/2$ in the isotropic chain). The Dedekind theta functions $\theta_n(u, q)$ should be taken as θ_2 for odd, and θ_3 for even chains. The amplitude prefactor A_z is non-universal (we also omit its weak temperature dependence due to logarithmic corrections).

The remaining ingredient is the partial derivative $\partial_x \theta_1(0, e^{-\frac{\pi\gamma}{2}}) \equiv \frac{\partial \theta_1(u, q)}{\partial u} |_{u=0}$.

So-defined segment susceptibility is then used to get the mean staggered susceptibility value by averaging over the length distribution:

$$\langle \chi_\pi^\pm(T, z) \rangle = \sum_L \chi_\pi^\pm(L, T) z^2 L (1-z)^L. \quad (\text{S.26})$$

Then within the mean-field approximation the Neel temperature is given by:

$$\langle \chi_\pi^\pm(T_N, z) \rangle = \frac{1}{J} \quad (\text{S.27})$$

2. Dimensionless

Now we can reformulate the above to make the LT/v scaling apparent. We make the integration variables dimensionless: $\tilde{x} = x/L$, $\tilde{y} = y/L$ and $\tilde{\tau} = \tau T$. Hence $v\tau/L = \gamma\tilde{\tau}$, with $\gamma = v/LT$ being our dimensionless parameter of interest. Then the susceptibility is:

$$\chi_\pi^\pm(L, T) = 2 \frac{A_z}{T} F_{1/2}^{e,o}(\gamma) \quad (\text{S.28})$$

where

$$F_{1/2}^{e,o}(\gamma) = \frac{\pi}{4} \int_0^1 \int_0^1 \int_0^1 \mathcal{G}_{1/2,\gamma}(\tilde{x}, \tilde{y}, \tilde{\tau}) d\tilde{x} d\tilde{y} d\tilde{\tau}$$

and the function $\mathcal{G}_{1/2,\gamma}$ being:

$$\mathcal{G}_{1/2,\gamma}(\tilde{x}, \tilde{y}, \tilde{\tau}) = \frac{\partial_x \theta_1(0, e^{-\frac{\pi\gamma}{2}})}{\sqrt{\theta_1(\pi\tilde{x}, e^{-\frac{\pi\gamma}{2}}) \theta_1(\pi\tilde{y}, e^{-\frac{\pi\gamma}{2}})}} [\mathcal{G}^+(\tilde{x}, \tilde{y}, \tilde{\tau}) - \mathcal{G}^-(\tilde{x}, \tilde{y}, \tilde{\tau})] \quad (\text{S.29})$$

$$\mathcal{G}^+(\tilde{x}, \tilde{y}, \tilde{\tau}) = \frac{\theta_{2,3}(\pi(\tilde{x} - \tilde{y}), e^{-\pi\gamma})}{\theta_{2,3}(0, e^{-\pi\gamma})} \sqrt{\frac{\theta_1(\frac{\pi(\tilde{x} + \tilde{y} + i\gamma\tilde{\tau})}{2}, e^{-\frac{\pi\gamma}{2}}) \theta_1(\frac{\pi(\tilde{x} + \tilde{y} - i\gamma\tilde{\tau})}{2}, e^{-\frac{\pi\gamma}{2}})}{\theta_1(\frac{\pi(\tilde{x} - \tilde{y} + i\gamma\tilde{\tau})}{2}, e^{-\frac{\pi\gamma}{2}}) \theta_1(\frac{\pi(\tilde{x} - \tilde{y} - i\gamma\tilde{\tau})}{2}, e^{-\frac{\pi\gamma}{2}})}} \quad (\text{S.30})$$

$$\mathcal{G}^-(\tilde{x}, \tilde{y}, \tilde{\tau}) = \frac{\theta_{2,3}(\pi(\tilde{x} + \tilde{y}), e^{-\pi\gamma})}{\theta_{2,3}(0, e^{-\pi\gamma})} \sqrt{\frac{\theta_1(\frac{\pi(\tilde{x} - \tilde{y} + i\gamma\tilde{\tau})}{2}, e^{-\frac{\pi\gamma}{2}}) \theta_1(\frac{\pi(\tilde{x} - \tilde{y} - i\gamma\tilde{\tau})}{2}, e^{-\frac{\pi\gamma}{2}})}{\theta_1(\frac{\pi(\tilde{x} + \tilde{y} + i\gamma\tilde{\tau})}{2}, e^{-\frac{\pi\gamma}{2}}) \theta_1(\frac{\pi(\tilde{x} + \tilde{y} - i\gamma\tilde{\tau})}{2}, e^{-\frac{\pi\gamma}{2}})}} \quad (\text{S.31})$$

Here e, o are standing for the cases of even or odd length (and thus θ_3 or θ_2 functions in (S.30, S.31)).

Having these function tabulated is the key to the calculation.

B. Generalization to the anisotropic case

1. Our assumptions

Transverse and longitudinal staggered susceptibilities for anisotropic Luttinger liquid in the magnetic field at

$\omega = 0$ are known to be [11]:

$$\chi^{zz}(q, T) = \frac{A_z}{4} [\Phi_K(q - \pi(1 - 2m), T) + \Phi_K(q - \pi(1 + 2m), T)] + \frac{1}{4\pi} \Xi_K(q), \quad (\text{S.32})$$

$$\chi^\pm(q, T) = A_x \Phi_{1/4K}(q - \pi, T). \quad (\text{S.33})$$

Here m is the magnetization in relative units, q is the momentum, K is the Luttinger parameter. The exact representation of Φ_K and Ξ_K functions is of no importance for the discussion below.

A key observation can be made from the generalized susceptibility definitions (S.32,S.33). For $m = 0$ and $q = \pi$ one has the longitudinal staggered susceptibility $\chi^{zz}(T) = \frac{A_z}{2} \Phi_K(0, T)$. At the same time, for arbitrary magnetization m and $q = \pi$ the transverse staggered susceptibility has a very similar form $\chi^\pm(T) = A_x \Phi_{1/4K}(0, T)$. Another term $\Xi_K(q)$ is irrelevant close to $q = \pi$. From this follows our **assumption 1**: *the staggered transverse susceptibility of a magnetized TLL with open boundary conditions $\chi_\pi^\pm = A_x f(L, T, \frac{1}{4K})$, where $f(L, T, K) = 2\chi_\pi^{zz}/A_z$ defines the staggered longitudinal susceptibility of zero-field TLL with the same Luttinger exponent K and velocity v .* Thus, in a case we have a formula for the finite-size zero field longitudinal susceptibility at hand, it can be easily converted to the formula

for transverse susceptibility of a magnetized system.

In principle, our assumption only states the simplest possible form of the transverse susceptibility, that is compatible with the condition $\chi_\pi^{xx} = \chi_\pi^{zz}$ for the finite-size isotropic system. However, more complicated scenarios are imaginable, for instance $f(L, T, K) = 2\chi_\pi^{zz}/A_z$ and $\chi_\pi^\pm/A_x = f(L\zeta(K), T, \frac{1}{4K})$ with $\zeta(1/2) = 1$. In principle, such renormalization of length might be the reason for the ‘‘horizontal’’ mismatch between the numeric and analytical results in Fig. 4 of the present Supplement.

A calculation for the anisotropic zero-field case does exist. An approximate Green function for the longitudinal staggered susceptibility of the XXZ chain can be found in the recent paper [12]. This function is written for the limit $\gamma \rightarrow \infty$ — finite chains and small temperatures (i.e. difference between the even and odd case is always going to be dramatic). The analogues of functions (S.23,S.24,S.25) are:

$$G(x, y, \tau) = \frac{A_z}{2} \left(\frac{4L^2}{\pi^2} \sin \frac{\pi x}{L} \sin \frac{\pi y}{L} \right)^{-K} [G^+(x, y, \tau) - G^-(x, y, \tau)] \quad (\text{S.34})$$

$$G^\pm(x, y, \tau) = \left(\frac{\sin \frac{\pi(x+y+i\tau)}{2L} \sin \frac{\pi(x+y-i\tau)}{2L}}{\sin \frac{\pi(x-y+i\tau)}{2L} \sin \frac{\pi(x-y-i\tau)}{2L}} \right)^{\pm K} \phi_\pm(x, y). \quad (\text{S.35})$$

$$\phi_\pm(x, y) = \cos \left(\frac{\pi(x \mp y)}{L} \right) \text{ for odd, 1 for even.}$$

Correspondingly, the dimensionless versions of Eqs. (S.34,S.35) are:

$$\begin{aligned} G(\tilde{x}, \tilde{y}, \tilde{\tau}) &= \frac{A_z}{2} \left(\frac{2L}{\pi} \right)^{-2K} (\sin \pi \tilde{x} \sin \pi \tilde{y})^{-K} [\mathcal{G}^+(\tilde{x}, \tilde{y}, \tilde{\tau}) - \mathcal{G}^-(\tilde{x}, \tilde{y}, \tilde{\tau})] \\ \mathcal{G}^\pm(x, y, \tau) &= \left(\frac{\sin \frac{\pi(\tilde{x}+\tilde{y}+i\gamma\tilde{\tau})}{2} \sin \frac{\pi(\tilde{x}+\tilde{y}-i\gamma\tilde{\tau})}{2}}{\sin \frac{\pi(\tilde{x}-\tilde{y}+i\gamma\tilde{\tau})}{2} \sin \frac{\pi(\tilde{x}-\tilde{y}-i\gamma\tilde{\tau})}{2}} \right)^{\pm K} \varphi_\pm(\tilde{x}, \tilde{y}) \\ \varphi_\pm(\tilde{x}, \tilde{y}) &= \cos \pi(\tilde{x} \mp \tilde{y}) \text{ for odd, 1 for even.} \end{aligned} \quad (\text{S.36})$$

Here comes our **assumption 2**, based on the limiting properties of θ - functions and the known isotropic case solution. *We propose the following generalization of terms in (S.36) for arbitrary γ :*

$$\begin{aligned}
\cos \pi(\tilde{x} \mp \tilde{y}) \text{ for odd, 1 for even} &\Rightarrow \frac{\theta_{2,3}(\pi(\tilde{x} \mp \tilde{y}), e^{-\frac{\pi\gamma}{2K}})}{\theta_{2,3}(0, e^{-\frac{\pi\gamma}{2K}})}, \\
\left(\frac{\sin \frac{\pi(\tilde{x}+\tilde{y}+i\gamma\tilde{\tau})}{2} \sin \frac{\pi(\tilde{x}+\tilde{y}-i\gamma\tilde{\tau})}{2}}{\sin \frac{\pi(\tilde{x}-\tilde{y}+i\gamma\tilde{\tau})}{2} \sin \frac{\pi(\tilde{x}-\tilde{y}-i\gamma\tilde{\tau})}{2}} \right)^{\pm K} &\Rightarrow \left(\frac{\theta_1\left(\frac{\pi(\tilde{x}+\tilde{y}+i\gamma\tilde{\tau})}{2}, e^{-\frac{\pi\gamma}{2}}\right)\theta_1\left(\frac{\pi(\tilde{x}+\tilde{y}-i\gamma\tilde{\tau})}{2}, e^{-\frac{\pi\gamma}{2}}\right)}{\theta_1\left(\frac{\pi(\tilde{x}-\tilde{y}+i\gamma\tilde{\tau})}{2}, e^{-\frac{\pi\gamma}{2}}\right)\theta_1\left(\frac{\pi(\tilde{x}-\tilde{y}-i\gamma\tilde{\tau})}{2}, e^{-\frac{\pi\gamma}{2}}\right)} \right)^{\pm K} \\
(\sin \pi\tilde{x} \sin \pi\tilde{y})^{-K} &\Rightarrow \left(\frac{\theta_1(\pi\tilde{x}, e^{-\frac{\pi\gamma}{2}})\theta_1(\pi\tilde{y}, e^{-\frac{\pi\gamma}{2}})}{[\partial_x \theta_1(0, e^{-\frac{\pi\gamma}{2}})]^2} \right)^{-K}
\end{aligned} \tag{S.37}$$

The Green function in question was not derived rigorously, so (S.37) should be considered as some sort of *ansatz*. For $K = 1/2$ case this recovers Eqs. (S.29, S.30, S.31) verbatim. The left-hand side is the correct $\gamma \rightarrow \infty$ limit of the right-hand side.

2. Universal scaling

Hence, from our assumptions 1 and 2 we can conclude that the staggered transverse susceptibility per TLL site has the following universal form (with all the SI factors now recovered):

$$\chi_\pi^\pm(L, T) = (g\mu_B)^2 \frac{A_x}{k_B v} \left(\frac{T}{v}\right)^{1/2K-2} F_K^{e,o} \left(\frac{v}{LT}\right), \tag{S.38}$$

where

$$F_K^{e,o}(\gamma) = \frac{1}{2} \gamma^{1/2K-1} \left(\frac{\pi}{2}\right)^{1/2K} \int_0^1 \int_0^1 \int_0^1 \mathcal{G}_{K,\gamma}(\tilde{x}, \tilde{y}, \tilde{\tau}) d\tilde{x} d\tilde{y} d\tilde{\tau}, \tag{S.39}$$

$$\begin{aligned}
\mathcal{G}_{K,\gamma}(\tilde{x}, \tilde{y}, \tilde{\tau}) &= \left(\frac{\theta_1(\pi\tilde{x}, e^{-\frac{\pi\gamma}{2}})\theta_1(\pi\tilde{y}, e^{-\frac{\pi\gamma}{2}})}{[\partial_x \theta_1(0, e^{-\frac{\pi\gamma}{2}})]^2} \right)^{-1/4K} \times \\
&\left\{ \frac{\theta_{2,3}(\pi(\tilde{x} - \tilde{y}), e^{-2K\pi\gamma})}{\theta_{2,3}(0, e^{-2K\pi\gamma})} \left(\frac{\theta_1\left(\frac{\pi(\tilde{x}+\tilde{y}+i\gamma\tilde{\tau})}{2}, e^{-\frac{\pi\gamma}{2}}\right)\theta_1\left(\frac{\pi(\tilde{x}+\tilde{y}-i\gamma\tilde{\tau})}{2}, e^{-\frac{\pi\gamma}{2}}\right)}{\theta_1\left(\frac{\pi(\tilde{x}-\tilde{y}+i\gamma\tilde{\tau})}{2}, e^{-\frac{\pi\gamma}{2}}\right)\theta_1\left(\frac{\pi(\tilde{x}-\tilde{y}-i\gamma\tilde{\tau})}{2}, e^{-\frac{\pi\gamma}{2}}\right)} \right)^{1/4K} - \right. \\
&\left. \frac{\theta_{2,3}(\pi(\tilde{x} + \tilde{y}), e^{-2K\pi\gamma})}{\theta_{2,3}(0, e^{-2K\pi\gamma})} \left(\frac{\theta_1\left(\frac{\pi(\tilde{x}+\tilde{y}+i\gamma\tilde{\tau})}{2}, e^{-\frac{\pi\gamma}{2}}\right)\theta_1\left(\frac{\pi(\tilde{x}+\tilde{y}-i\gamma\tilde{\tau})}{2}, e^{-\frac{\pi\gamma}{2}}\right)}{\theta_1\left(\frac{\pi(\tilde{x}-\tilde{y}+i\gamma\tilde{\tau})}{2}, e^{-\frac{\pi\gamma}{2}}\right)\theta_1\left(\frac{\pi(\tilde{x}-\tilde{y}-i\gamma\tilde{\tau})}{2}, e^{-\frac{\pi\gamma}{2}}\right)} \right)^{-1/4K} \right\}.
\end{aligned} \tag{S.40}$$

The power law $T^{\frac{1}{2K}-2}$ is the key result. It also matches the infinite length limit power law for the staggered susceptibility [4, 11]:

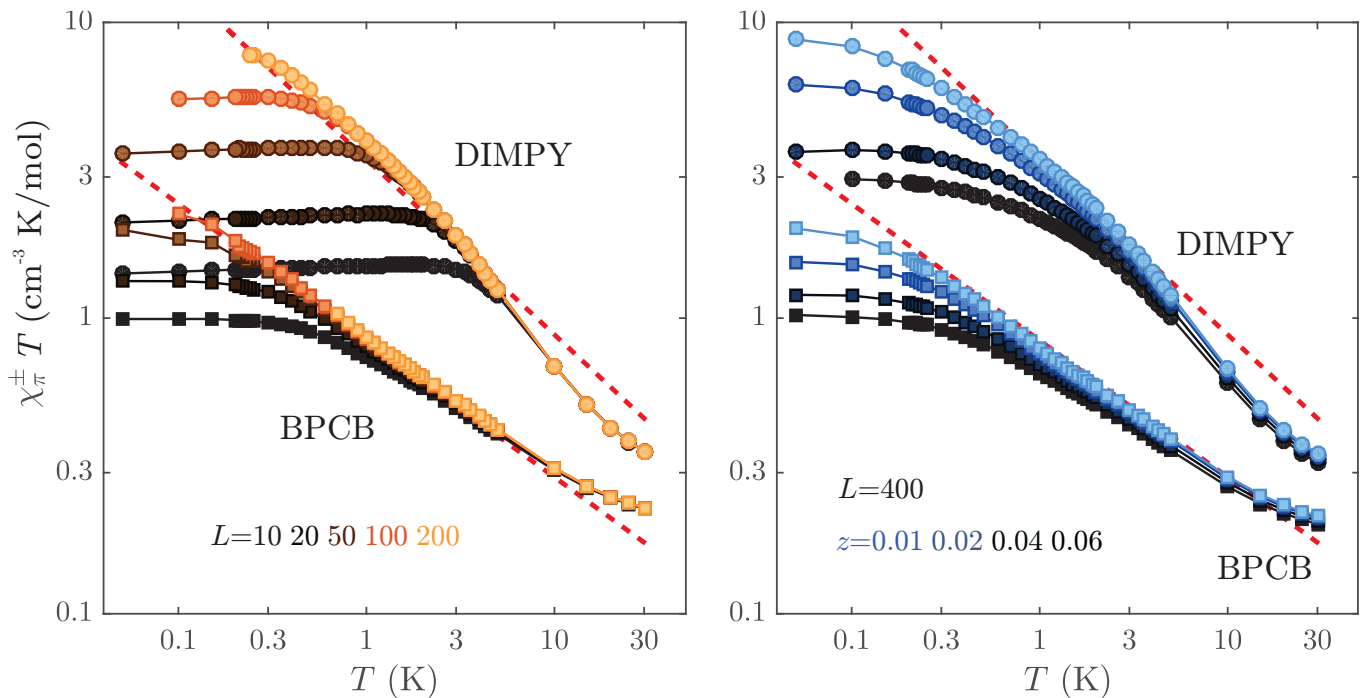
$$\chi_\pi^\pm(T) = (g\mu_B)^2 \frac{A_x}{k_B v} \left(\frac{T}{v}\right)^{1/2K-2} \times \left[\frac{1}{2} (2\pi)^{1/2K-2} \sin\left(\frac{\pi}{4K}\right) B^2 \left(\frac{1}{8K}, 1 - \frac{1}{4K}\right) \right]. \tag{S.41}$$

VI. UNIVERSAL SUSCEPTIBILITY VS NUMERICS AND EXPERIMENT

In this section we will compare the previously developed analytical ansatz with the results of QMC calculations.

A. The QMC data and the pristine TLL description

In Fig. 3 the staggered susceptibility versus temperature is displayed for all the types of ladders considered: both BPCB and DIMPY at 8 T, in shorter finite-segment (10 – 200 rungs) and depleted long segment (400 rungs) settings. This data can be compared to the expectations



SUPP. FIG. 3. The QMC susceptibility data for DIMPY and BPCB. In the left panel the data for the finite-size ladder segments is shown; in the right panel — for the long segments with depletion z . Dashed lines show the TLL result for the clean infinite system.

for the corresponding pristine TLL model. One can see that in all the cases the “paramagnetic” regime at high temperatures is followed by the part that matches the $L = \infty$ TLL behavior (S.41) well. This temperature window gets shorter as the segment size is decreased or more disorder is added, and at low T the “finite-size” behavior starts to dominate the susceptibility.

B. Scaled QMC data and the scaling ansatz

The results can further be compared to the predictions of LT/v scaling behavior. The key result of our ansatz is contained in Eqs. (S.38-S.40). These functions for both BPCB and DIMPY cases are plotted along with the data for the finite-size segments and for the long depleted segments. We can see in Fig. 4 that in general the behavior of the scaled staggered susceptibility is in the quantitative agreement with the theoretical predictions. However, there is a number of discrepancies.

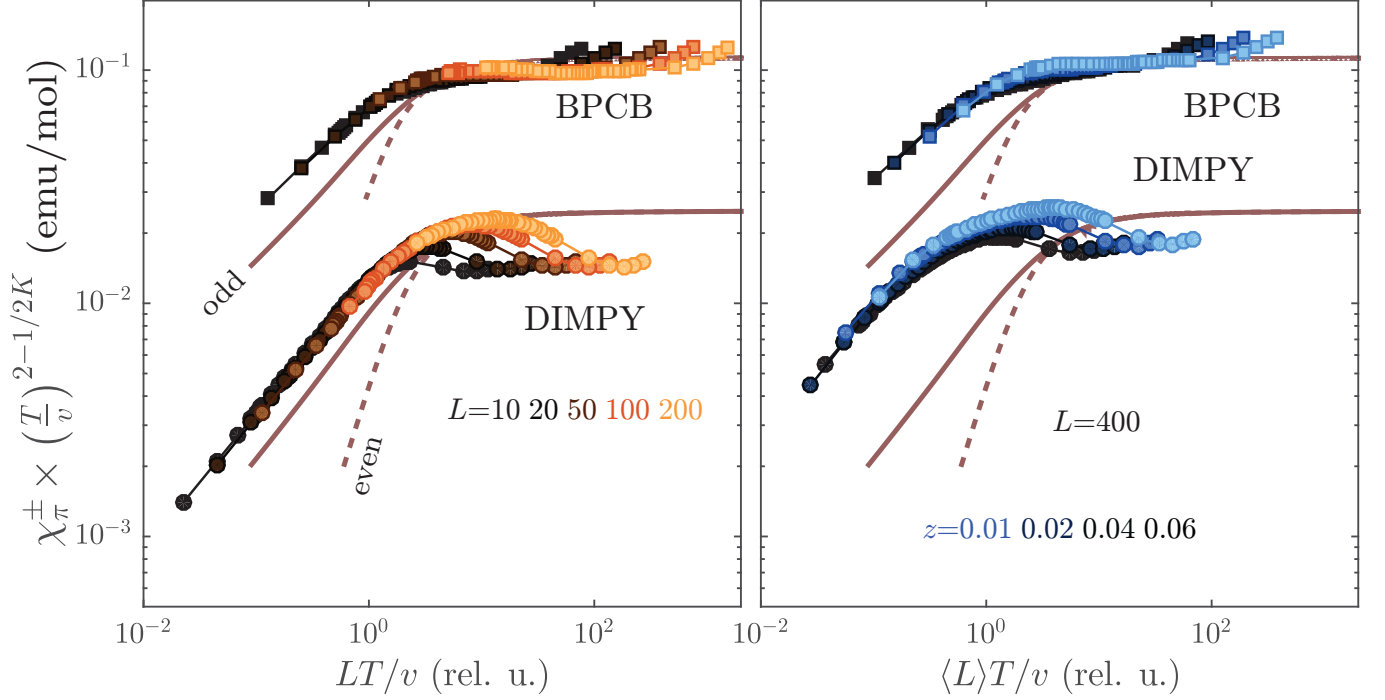
First, only the “odd” version of the scaling function $F_K(\gamma)$ (S.39) seems to be relevant to the data. This is understood as a consequence of extracting the $\chi_\pi^\pm(T)$ in an indirect way from the equal-time correlations. The latter quantity does not display an even-odd sensitivity, so neither does the obtained susceptibility.

Second, in the shorter finite-sized segments we see an offset in LT/v , by the factor of 2 roughly. This offset seems to be the same for both DIMPY and BPCB datasets. The reason for that is not understood now.

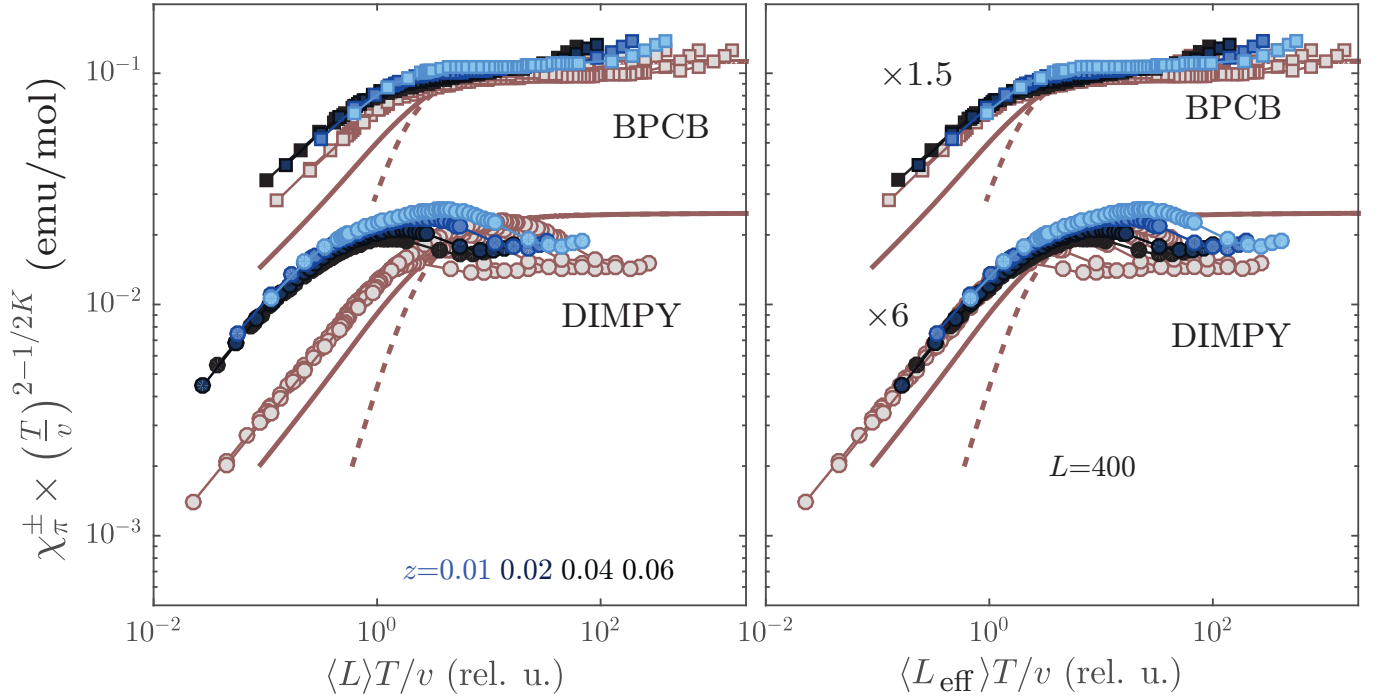
Third, we see a much more significant offset in the depleted ladders datasets. This time the offset *does* depend on the particular ladder (DIMPY or BPCB), being much stronger for the strong-leg case, as the Fig. 5 shows. We understand it as the effect of the partial defect transparency discussed in the main text. This partial transparency means that the effective length has to be renormalized: it is not merely a mean distance between the defects but some longer effective scale. Naturally, this effect is much stronger for the case of DIMPY (where the defects are very transparent), while in BPCB this renormalization is insignificant compared to the bare segment case. As Fig. 5 shows, for BPCB the length renormalization factor is mere 1.5, while it is 6 for DIMPY.

C. The scaling ansatz and the measured phase diagrams

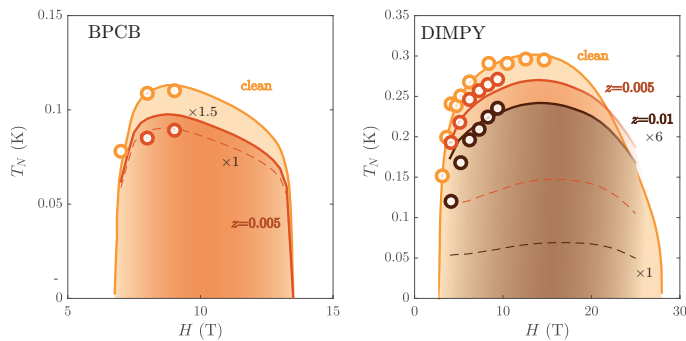
Since the scaling predictions are in a good agreement with the predictions of the numerical simulations, one can try to predict the depleted ladder phase diagram in “bruteforce” manner, based only on the known field dependencies of K , v and A_x . The susceptibility of an infinite depleted ladder can be obtained from taking the distribution of the segment length into account for a given z . An empirical correction factor for the effective length discussed in the previous section can also be included. Then, susceptibility of an individual segment of a given length can be obtained with the Eqs. (S.38-S.40). Thus,



SUPP. FIG. 4. Scaled QMC data for DIMPY and BPCB versus Eqs. (S.38-S.40). In the left panel the data for the finite-size ladder segments is shown; in the right panel — for the long segments with depletion z . The analytical curves are identical in both cases. Solid line stands for the odd version of Eqs. (S.38-S.40), and dashed line for the even one.



SUPP. FIG. 5. Comparison of the scaled datasets for the depleted ladders and finite-sized segments. The latter are shown in the background together with the analytical ansatz curves. In the left panel the data is shown “as is”, and in the right panel the average impurity-impurity distance is enlarged by the effective factor λ_{eff} (1.5 for BPCB, 6 for DIMPY).



SUPP. FIG. 6. Experimental data vs TLL scaling-based approach for DIMPY and BPCB. The color coding is the same as in Fig. 5 from the main text; the experimental data points are also identical. Solid lines stand for the theoretical calculation (S.42) taking the λ_{eff} into account (as also indicated on the plot). Dashed lines show the result that does not include this renormalization correction. The “clean” lines is the infinite system TLL result, known from the literature.

the susceptibility of the depleted ladder per mol of spins is:

$$\chi_{\pi}^{\pm}(z, T) = N_A \sum_L \rho_z(L) \chi_{\pi}^{\pm}(L \lambda_{\text{eff}}, T). \quad (\text{S.42})$$

with λ_{eff} being the parameter, describing the effective length of the segment between the two impurities at distance L from each other, The probability of finding such segment is given by:

$$\rho_z(L) = L(2z)^2(1 - 2z)^L. \quad (\text{S.43})$$

Using the known $T_N(H)$ in the pristine TLL model and the field dependencies of effective TLL parameters as given Refs. [3, 4], we obtain the approximations of the phase boundaries shown in Fig. 6.

We see that overall the agreement between the analytical approximation and the observed phase boundaries is quite good. The λ_{eff} correction is rather marginal in case of BPCB. In case of DIMPY, however, it is absolutely crucial for obtaining the realistic result. We conclude that the approach based on the LT/v universality and the mean field ordering criterion works quite well for describing the phase diagrams of the depleted spin ladders.

-
- [1] A. W. Sandvik, Stochastic series expansion method with operator-loop update, *Phys. Rev. B* **59**, R14157 (1999).
- [2] B. Bauer, L. D. Carr, H. G. Evertz, A. Feiguin, J. Freire, S. Fuchs, L. Gamper, J. Gukelberger, E. Gull, S. Guertler, *et al.*, The ALPS project release 2.0: open source software for strongly correlated systems, *J. Stat. Mech. Theor. Exp.* **2011**, P05001 (2011).
- [3] D. Schmidiger, P. Bouillot, S. Mühlbauer, S. Gvasaliya, C. Kollath, T. Giamarchi, and A. Zheludev, Spectral and Thermodynamic Properties of a Strong-Leg Quantum Spin Ladder, *Phys. Rev. Lett.* **108**, 167201 (2012).
- [4] P. Bouillot, C. Kollath, A. M. Läuchli, M. Zvonarev, B. Thielemann, C. Rüegg, E. Orignac, R. Citro, M. Klanjšek, C. Berthier, M. Horvatić, and T. Giamarchi, Statics and dynamics of weakly coupled antiferromagnetic spin- $\frac{1}{2}$ ladders in a magnetic field, *Phys. Rev. B* **83**, 054407 (2011).
- [5] V. N. Glazkov, M. Fayzullin, Y. Krasnikova, G. Skoblin, D. Schmidiger, S. Mühlbauer, and a. Zheludev, ESR study of the spin ladder with uniform Dzyaloshinskii-Moria interaction, **184403**, 1 (2015), arXiv:1507.02503.
- [6] B. R. Patyal, B. L. Scott, and R. D. Willett, Crystal-structure, magnetic-susceptibility, and EPR studies of bis(piperidinium)tetrabromocuprate(II): A novel monomer system showing spin diffusion, *Phys. Rev. B* **41**, 1657 (1990).
- [7] D. Schmidiger, K. Yu. Povarov, S. Galeski, N. Reynolds, R. Bewley, T. Guidi, J. Ollivier, and A. Zheludev, Emergent Interacting Spin Islands in a Depleted Strong-Leg Heisenberg Ladder, *Phys. Rev. Lett.* **116**, 257203 (2016).
- [8] A. Lavarélo, G. Roux, and N. Laflorencie, Magnetic responses of randomly depleted spin ladders, *Phys. Rev. B* **88**, 134420 (2013).
- [9] G. Simutis, S. Gvasaliya, M. Månsson, A. L. Chernyshev, A. Mohan, S. Singh, C. Hess, A. T. Savici, A. I. Kolesnikov, A. Piovano, T. Perring, I. Zaliznyak, B. Büchner, and A. Zheludev, Spin Pseudogap in Ni-Doped SrCuO₂, *Phys. Rev. Lett.* **111**, 067204 (2013).
- [10] S. Eggert, I. Affleck, and M. D. P. Horton, Néel Order in Doped Quasi-One-Dimensional Antiferromagnets, *Phys. Rev. Lett.* **89**, 047202 (2002).
- [11] T. Giamarchi, *Quantum Physics in One Dimension* (Oxford University Press, 2003).
- [12] A. Bohrdt, K. Jägering, S. Eggert, and I. Schneider, Dynamic structure factor in impurity-doped spin chains, *Phys. Rev. B* **98**, 020402 (2018).